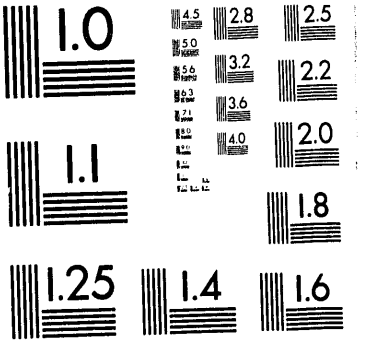
1.0
4.5
2.8
2.5
5.0
5.6
3.2
2.2
6.3
7.1
3.6
8.0
4.0
2.0
1.1
1.8
1.25
1.4
1.6

1 of 1

DOE/PC/91309--T9

HIGH TEMPERATURE ALKALI CORROSION OF CERAMICS

IN COAL GAS

DE-FG22-91PC91309

Quarterly Progress Report #8
for the Period
June 1, 1993 - September 1, 1993

Prepared by

G.R. Pickrell, T. Sun, and J.J. Brown

Center for Advanced Ceramic Materials
Virginia Polytechnic Institute
and State University
Blacksburg, VA 24061

Prepared for

Department of Energy
Pittsburgh Energy Technology Center
P.O. Box 10940
Pittsburgh, Pennsylvania 15236

August 24, 1993

DISCLAIMER

This report was prepared as an account of work sponsored by an agency of the United States Government. Neither the United States Government nor any agency thereof, nor any of their employees, makes any warranty, express or implied, or assumes any legal liability or responsibility for the accuracy, completeness, or usefulness of any information, apparatus, product, or process disclosed, or represents that its use would not infringe privately owned rights. Reference herein to any specific commercial product, process, or service by trade name, trademark, manufacturer, or otherwise does not necessarily constitute or imply its endorsement, recommendation, or favoring by the United States Government or any agency thereof. The views and opinions of authors expressed herein do not necessarily state or reflect those of the United States Government or any agency thereof.

"U.S. DOE Patent Clearance is not required prior to the publication of this document."

MASTER

DISTRIBUTION OF THIS DOCUMENT IS UNLIMITED

Summary

The gaseous alkali corrosion kinetics of Si_3N_4 were systematically investigated from 950 to 1100°C in an atmosphere containing 0.98 vol% sodium nitrate vapors. The linear reaction rates from 950 to 1100°C indicate that the alkali reaction of Si_3N_4 is interface-controlled with an activation energy of 199 kJ/mol. The rate controlling step of the overall reaction appears to be the oxidation of Si_3N_4 to SiO_2. The alkali reaction mechanism, which involved a complex dissolution-oxidation process, was proposed according to the reaction kinetics. The distinct difference between the oxidation of Si_3N_4 in air and the reaction of Si_3N_4 in the presence of alkali is the dissolution process of SiO_2 in the sodium silicate liquid.

The gaseous alkali corrosion kinetics of alumina were investigated at 1100°C and 1150°C. The reaction thickness is linearly related to the reaction time, suggesting an interface-controlled reaction mechanism. The reaction rate constants are 0.24 μm/h and 0.45 μm/h at 1100°C and 1150°C, respectively. The alumina grains seemed to be preferentially attacked along certain crystallographic directions.

The subsolidus phase relations in the Na_2O-Al_2O_3-TiO_2 system were studied. Phase analysis indicates that the Na_2O-Al_2TiO_6 section is not a true binary system. A revised phase diagram showing the subsolidus equilibria for the Na_2O-Al_2O_3-TiO_2 system was constructed according to additional experimental data.

Objective/Scope

High temperature alkali corrosion has been known to cause premature failure of ceramic components used in advanced high temperature coal combustion systems such as coal gasification and clean-up, coal fired gas turbines, and high efficiency heat engines. The objective of this research is to systematically evaluate the alkali corrosion resistance of the most commonly used structural ceramics including silicon carbide, silicon nitride, cordierite, mullite, alumina, aluminum titanate, zirconia, and fireclay glass. The study consists of identification of the alkali reaction products (phase equilibria) and the kinetics of the alkali reactions.

Technical Progress

I. Alkali Reaction Products

The subsolidus phase relations in the Na_2O-Al_2O_3-TiO_2 system were further verified for compositions between the $NaAlO_2$-$Na_8Ti_5O_{14}$ join and the Al_2O_3-TiO_2 join. The samples were prepared by repeatedly grinding and mixing appropriate amounts of aluminum oxide, titanium dioxide and sodium carbonate in an alumina mortar. The mixture was dried and fired at successively higher temperatures up to 1100°C in alumina crucibles. After each heat treatment, the samples were ground for x-ray diffraction analysis. The samples were weighed before and after each heat treatment to determine

if soda was lost during firing. The weight loss observed for each sample corresponds to the weight loss of carbon dioxide from the decomposition of sodium carbonate, even after firing up to 1100°C for 67 h. The phases formed after the heat treatments and the phase transition temperatures of the Na_2O-Al_2O_3-TiO_2 system were determined using x-ray diffraction (XRD) and differential thermal analysis (DTA), respectively.

Table 1 lists the compositions and the phase assemblages of the Na_2O-Al_2O_3-TiO_2 reaction at different temperatures. The formation of β-alumina at 840°C appears to be very sluggish. As a result, the alumina phase observed in samples 2, 3, and 4 at 840°C indicates that longer heat treatment is necessary to reach equilibrium. At higher temperatures, β-alumina was formed and the free alumina phase was not observed for the same compositions. Based on the phase analysis for the compositions studied, a phase diagram showing the subsolidus equilibria for the Na_2O-Al_2O_3-TiO_2 system was constructed as shown in Figure 1. An unknown ternary phase in the ternary system persisted after repeated grinding and firing up to 1100°C. The phase relations observed indicate that the composition of the unknown phase is likely to contain about 55% TiO_2, 39% Al_2O_3 and 6% Na_2O (in weight). The ternary compounds which were reported in literature, were not observed in any of the x-ray diffraction patterns for the samples fired in air. The phase assemblages indicate that the Na_2O-Al_2TiO_6 section is not a true binary system.

II. Alkali Corrosion Kinetics

(a) Silicon Nitride

The gaseous alkali corrosion kinetics of Si_3N_4 (Kyocera) were examined in a constant alkali vapor concentration from 950 to 1100°C. As mentioned in previous reports, the constant alkali vapor concentration was maintained by independently heating sodium nitrate at 715°C and monitoring the weight loss of the salt as a function of reaction time and temperature. The alkali vapors were transported to the reaction chamber by compressed air, which was filtered to remove moisture and carbon dioxide. The concentration of sodium nitrate was calculated to be approximately 0.98 vol%. The Si_3N_4 pellets (approximately 3x3x6 mm), which contain alumina as a sintering aid, were vertically placed in an alumina holder containing alumina powders to support the specimens and protect the back of the pellets from reaction. The specimens were isothermally heated between 950°C and 1100°C for 2 h to 15 h, followed by air-quenching. The thickness change of the Si_3N_4 pellets following exposures to the alkali containing atmosphere was measured according to the previously described procedure.

1. Reaction Kinetics

Figure 2 shows the thickness of the corrosion layer of Si_3N_4 as a function of reaction temperature and time. The data shown in Figure 2 are taken from the average reaction thickness of four specimens. As listed in Table 2, the alkali reaction rate of Si_3N_4 ranges

from 3.0 μm/h at 950°C to 27.2 μm/h at 1100°C. Figure 3 shows the Arrhenius plot of the rate constant versus temperature according to the equation $k = k_0 \exp(-Q/RT)$, where k represents the reaction rate. The activation energy associated with the alkali reaction is 199 kJ/mol. The linear relationship between the reaction thickness and time at all temperatures clearly indicates a reaction-controlled, instead of a diffusion-controlled, corrosion process of the Si_3N_4 in the presence of alkali vapors. The reaction-controlled process is further supported by the activation energy difference between Si_3N_4 and SiC. If the reaction is diffusion-controlled, the activation energy and the reaction rate should be the same for both Si_3N_4 and SiC, since both involve oxygen diffusion through sodium silicate liquids with approximately the same soda contents. Also note that above 950°C, the reaction of Si_3N_4 is faster than the reaction of SiC and the reverse is true at temperatures below 950°C, as shown in Figure 3. Figure 4 shows a comparison of the oxidation of Si_3N_4 in air and the alkali reaction of Si_3N_4 at 1100°C. Based on the calculation of reaction thickness, the reaction rate of Si_3N_4 in the alkali-containing atmosphere is approximately 10^4 times faster than the oxidation rate of Si_3N_4 in air at 1100°C. The accelerated reaction rate is attributed to the formation of a sodium silicate liquid, which allows oxygen to diffuse quickly to the interface of Si_3N_4 and the liquid. When the silica layer on the surface of Si_3N_4 is transformed to the sodium silicate liquid, the oxygen diffusivity is increased by approximately 10^6 times. The kinetic data presented in Figure 2 greatly help understand the reaction mechanism and the rate controlling step of the alkali corrosion of Si_3N_4.

2. Reaction Mechanism

Figure 5 depicts the oxidation of Si_3N_4 in air and the reaction of Si_3N_4 in the alkali-containing atmosphere. The oxidation of Si_3N_4 in air involves the adsorption of oxygen on the surface; the inward diffusion of oxygen through the SiO_2 and the Si_2N_2O layers; the oxidation at the SiO_2-Si_2N_2O and Si_3N_4-Si_2N_2O interfaces; and the outward diffusion of the gas product N_2 through the SiO_2 and Si_2N_2O layers. This oxidation process is sluggish because of the presence of the SiO_2 and the Si_2N_2O which serve as diffusion barriers for oxygen. In contrast, the rapid reaction rate of Si_3N_4 in the presence of alkali vapors, as shown in Figures 2 and 4, suggests that the protective SiO_2 and Si_2N_2O layers were no longer present, otherwise the reaction would be slow as in the case of the oxidation in pure air. In addition, the atomic absorption analysis of the Na/Si ratio for all the specimens soaked in HF solutions indicates that the average Na_2O content is about 31 mol%, which, according to the Na_2O-SiO_2 phase diagram (Figure 6), lies in the single liquid phase region and therefore forbids the precipitation of SiO_2. Assuming local equilibrium, the oxide (SiO_2) was readily dissolved in the sodium silicate liquid upon oxidation, and did not have sufficient time to grow. In this case, the alkali reaction of Si_3N_4 involves a complex dissolution-oxidation process, which can be categorized by (1) adsorption of alkali vapors on the surface of silica, (2) reaction of silica and alkali to form a sodium silicate liquid, (3) diffusion of oxygen through the liquid phase, (4) oxidation of oxynitride to silica, (5) dissolution of silica in the sodium silicate liquid, (6) oxidation of Si_3N_4 to silica, and (7) outward diffusion of product gas N_2. The distinct difference

between the two types of reaction shown in Figure 5 is the dissolution process of the silica which is responsible for the enhanced oxidation rate of Si_3N_4.

3. Rate Controlling Step

To identify the rate controlling step of the reaction, it is usually necessary to know the reaction rate of each step involved in the overall reaction. Most of the kinetic data associated with the step reactions discussed in the reaction mechanism section are not available. However, knowing the characteristics of each reaction involved in the overall reaction proves helpful. Since the alkali reaction of Si_3N_4 exhibits reaction-controlled characteristics (Figure 2), the diffusion of oxygen, as well as the outward diffusion of N_2, can be ruled out as the rate controlling step. Review of the literature indicates that the dissolution of silica in a variety of sodium silicate liquids followed the parabolic rate law; therefore, the dissolution of silica can not be the rate controlling step. The adsorption or the absorption of alkali in the sodium silicate liquid is not likely to be the rate controlling step either. The possible rate controlling step is, accordingly, the oxidation of Si_3N_4 to Si_2N_2O, the oxidation of Si_3N_4 to SiO_2, or the oxidation of Si_2N_2O to SiO_2. The linear reaction rate suggests that the Si_2N_2O layer is not present or does not have sufficient time to grow during the alkali reaction of Si_3N_4. The presence of Si_2N_2O implies that the oxidation of Si_3N_4 requires the diffusion of oxygen through the Si_2N_2O layer, making the overall reaction a diffusion-controlled process. Based on the characteristics of each step reaction and the kinetic data presented, it can be concluded that the rate controlling step

of the alkali reaction of Si_3N_4 is the oxidation of Si_3N_4 to SiO_2.

It should be pointed out that the initial stage of the alkali reaction of Si_3N_4 involves the removal of the protective SiO_2 layer which is a diffusion-controlled process (parabolic reaction). Because of the reaction time used in this study, the removal of the SiO_2 layer in the initial stage may be too fast to be detected.

4. Microstructure Analysis

Figure 7 shows the SEM micrographs of the fracture surface of the as-received specimen and the surface of the Si_3N_4 after a 19 h exposure at 1000°C in the alkali containing atmosphere. The grain boundaries appear to be preferentially attacked as evidenced by the well etched grains shown in the micrograph. This preferential attack may be caused by the segregation of the sintering aid at grain boundaries. The Si_3N_4 specimens used in this study contain alumina as a sintering aid. The morphology of the grains does not appear to have been affected by the alkali exposure.

(b) Alumina

The gaseous alkali corrosion kinetics of alumina (Coors) were also examined in the same alkali-containing atmosphere from 1100 to 1150°C. The reaction layer thickness versus reaction time is shown in Figure 8. The linearity of the thickness versus time plot indicates the reaction is interface-controlled. The reaction rate constants for 1100°C and 1150°C are 0.24 μm/h and 0.45 μm/h respectively. The reaction temperature was

increased to 1150°C in order to produce a measurable reaction layer in a reasonable period of time. The thickness change of the alumina pellet after alkali reaction at 1050°C for 48 hours was less than 5 microns. The alkali reaction rates for temperatures lower than 1050°C will not be measured in this study due to the prohibitively slow nature of the alkali reaction of alumina at these temperatures. The reaction rates for alumina appear to be much slower than those for the SiC or Si_3N_4. The microstructure of the alumina pellets before and after the alkali reaction is shown in Figure 9. There appears to be some preferential attack of the grains along certain crystallographic directions. EDX measurements on as-received alumina samples showed only Al was present and both Na and Al were detected after alkali reaction at 1150°C for 120 h. The only phases detected in the x-ray diffraction patterns of the samples reacted at 1100°C for 120 h were sodium aluminate and alumina. After etching in dilute HF, the only phase detected in the x-ray pattern was alumina. The kinetic data at 1050°C are being collected and the results will be included in the next report.

Table 1. Phase Analysis of the Soda-Aluminum Titanate System

Sample No.	Composition (wt%) Na_2O	Al_2O_3	TiO_2	Temp (°C)/ Time (h)	Observed Phases	Phase Transition Temperatures
1.	32	20	48			956
				840 / 72	NT_3 + N_4T_5 + NA	
				840 / 91	NT_3 + N_4T_5 + NA	
				840 / 119	NT_3 + N_4T_5 + NA	
				840 / 91	NT_3 + N_4T_5 + NA	
				940 / 46	NT_3 + NA + Liq	
2.	20	35	45			991
				840 / 72	NT_3 + NA + A	1046
				840 / 91	NT_3 + NA + A	1070
				840 / 119	NT_3 + NA + A	
				840 / 91	NT_3 + NA + A	
				940 / 46	NT_3 + NA + βA	
				1000 / 16	NT_3 + NA + βA	
				1100 / 67	βA + X + Liq	
3.	40	30	30			991
				840 / 72	NT_3 + NA + A	1046
				840 / 91	NT_3 + NA + A	1070
				840 / 119	NT_3 + NA + A	
				840 / 91	NT_3 + NA + A	
				940 / 46	NT_3 + NA + βA	
				1000 / 16	NT_3 + NA + βA	
				1100 / 67	βA + X + Liq	
4.	18	69	13			999
				840 / 72	NT_3 + NA + A	1040
				840 / 91	NT_3 + NA + A + βA	
				840 / 119	NT_3 + NA + A + βA	
				840 / 91	NT_3 + NA + A + βA	
				940 / 46	NT_3 + NA + βA	
				1000 / 16	NT_3 + NA + βA	
				1100 / 67	βA + NA + Liq	

Sample No.	Composition (wt%) Na_2O	Al_2O_3	TiO_2	Temp (°C)/ Time (h)	Observed Phases	Phase Transition Temperatures
5.	4	84	12			1037
				840 / 72	$NT_3 + \beta A + A$	
				840 / 91	$NT_3 + \beta A + A$	
				840 / 119	$NT_3 + \beta A + A$	
				840 / 91	$NT_3 + \beta A + A$	
				940 / 46	$NT_3 + \beta A + A$	
				1000 / 16	$NT_3 + \beta A + A$	
				1100 / 67	$\beta A + A$ + Liq	
6.	2	45	53			none
				840 / 72	A + T + X	
				840 / 91	A + T + X	
				840 / 119	A + T + X	
				840 / 91	A + T + X	
				940 / 46	A + T + X	
				1000 / 16	A + T + X	
				1100 / 67	A + T + X	
7.	9	15	76			none
				840 / 72	NT_6 + T(tr) + X	
				840 / 91	NT_6 + T(tr) + X	
				840 / 119	NT_6 + T(tr) + X	
				840 / 91	NT_6 + T(tr) + X	
				940 / 46	NT_6 + T(tr) + X	
				1000 / 16	NT_6 + T(tr) + X	
				1100 / 67	X + Liq	

NA = $NaAlO_2$, bA = $NaAl_{11}O_{17}$, NT_3 = $Na_2Ti_3O_7$, NT_6 = $Na_2Ti_6O_{13}$, N_4T_5 = $Na_8Ti_5O_{14}$, A = Al_2O_3, T = TiO_2, X = unknown ternary phase

Table 2. Alkali Reaction Kinetics of Si_3N_4 and Chemical Analysis of Sodium Silicate Liquids

Temp (°C)	Reaction rate (μm)
950	3.00
1000	7.40
1050	12.95
1100	27.22
Activation energy:	199 kJ/mol
Average SiO_2/Na_2O molar ratio:	2.22 ± 0.64

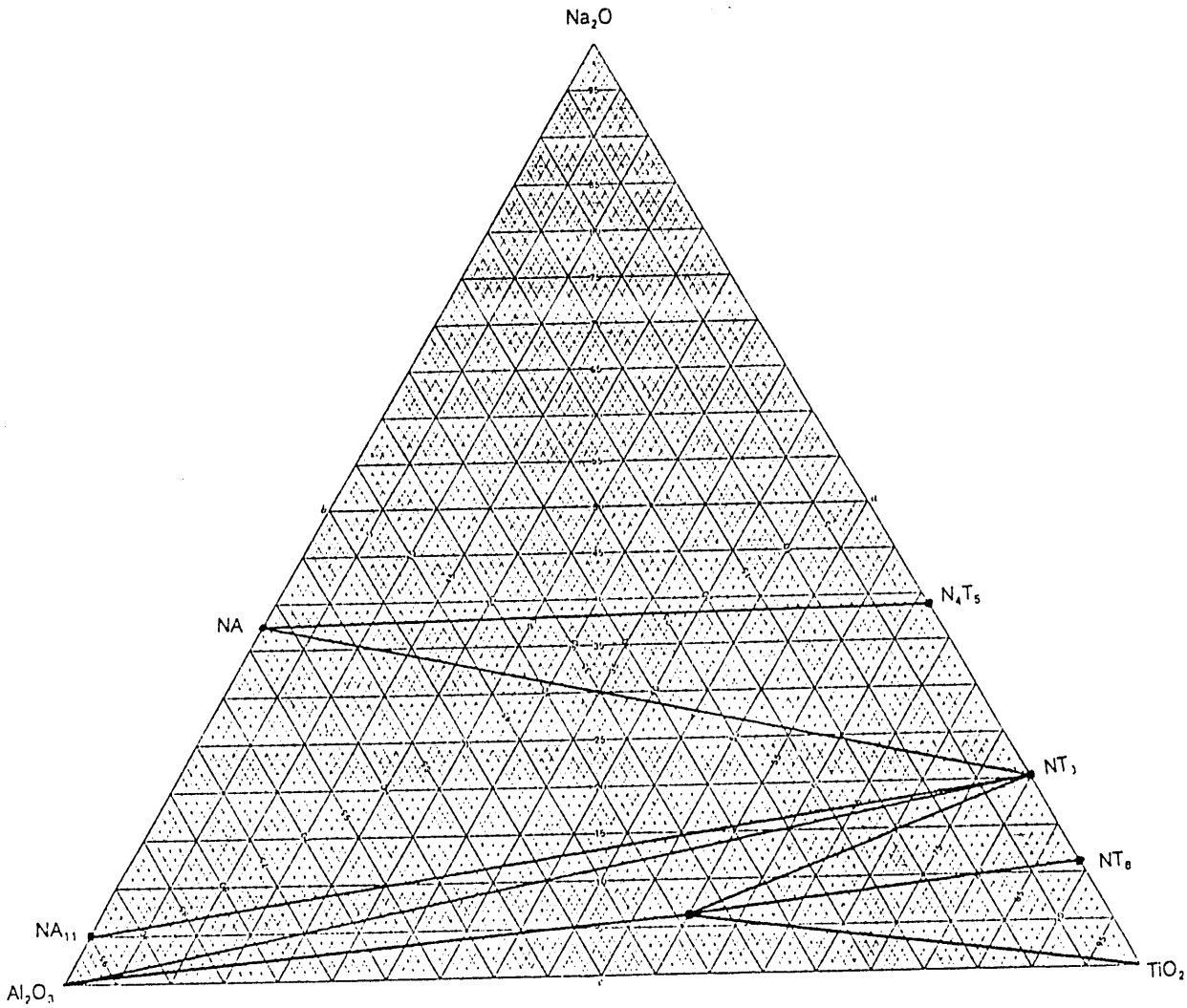

Figure 1. Subsolidus phase equilibria in the Na_2O-Al_2O_3-TiO_2 system

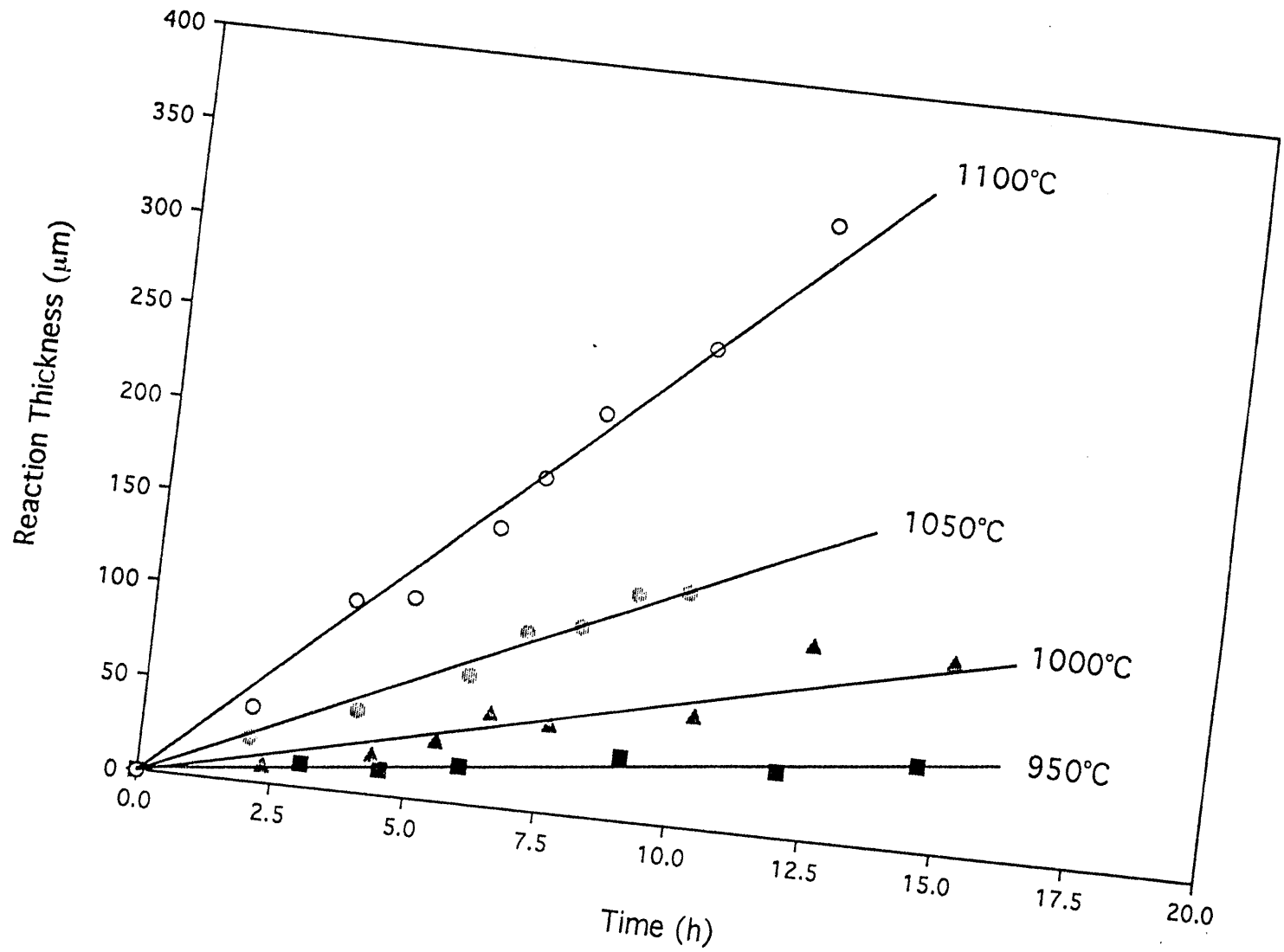

Figure 2. Corrosion thickness of Si_3N_4 as a function of temperature and time.

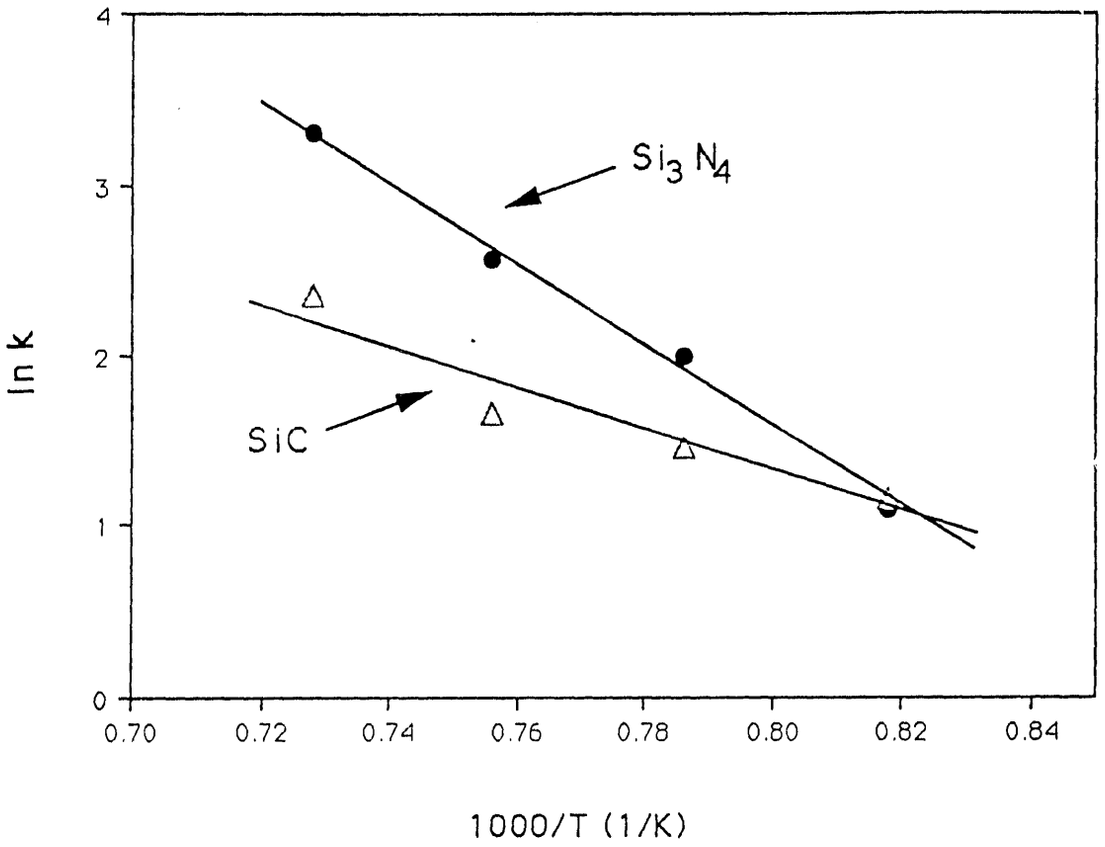

Figure 3. Arrhenius plot of rate constant versus temperature for Si_3N_4 and SiC.

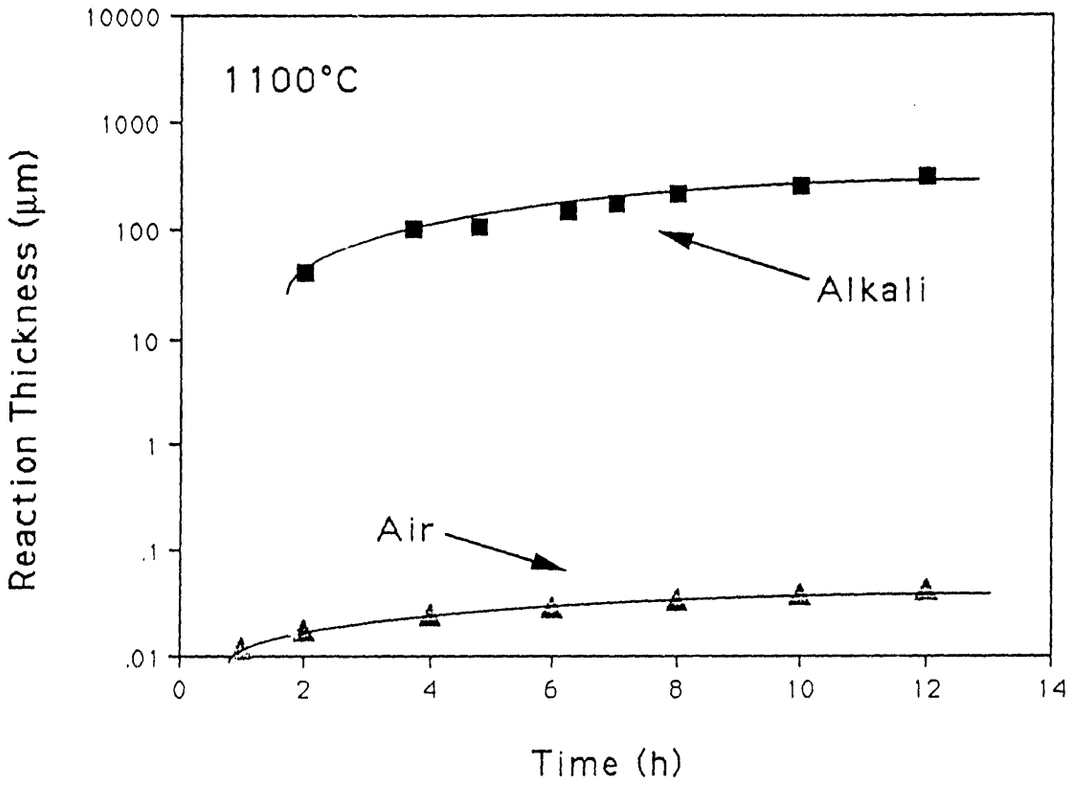

Figure 4. Comparison of oxidation of Si_3N_4 in air and in alkali-containing atmosphere at 1100°C; data in air were taken from literature.

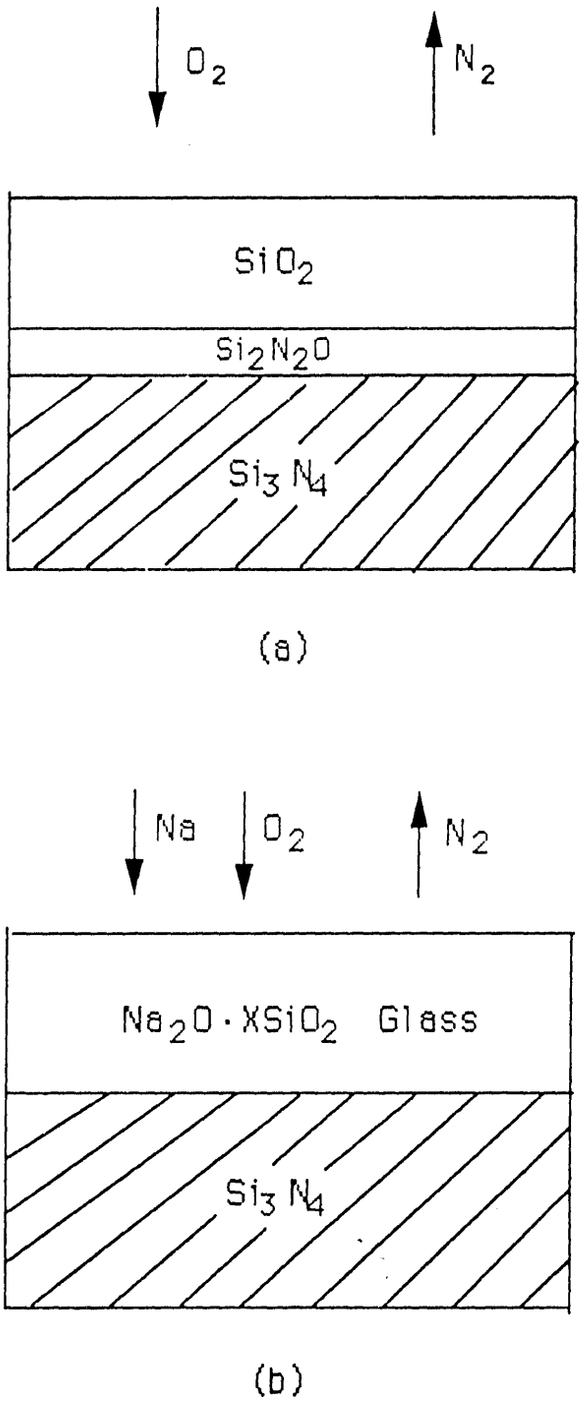

Figure 5. Schematic of oxidation of Si_3N_4 in (a) dry air, and (b) dry air containing Na vapor, where x = 2.22.

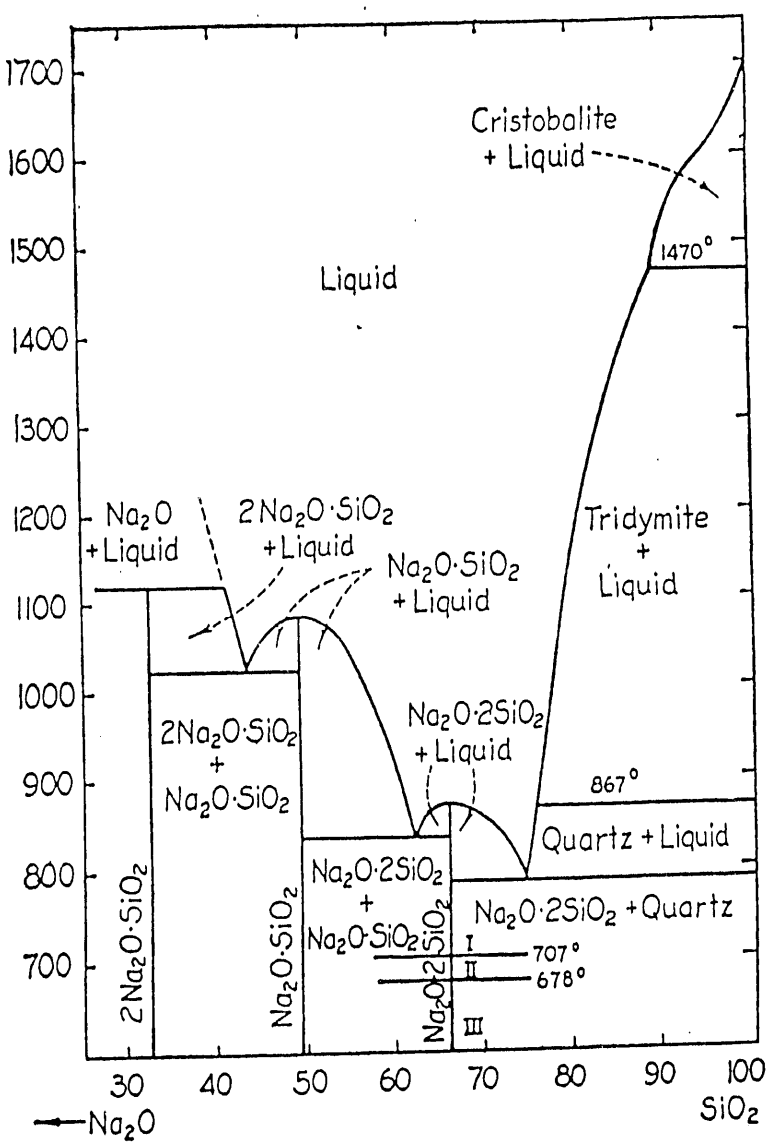

Figure 6. Phase diagram of the Na_2O-SiO_2 system.

a.)

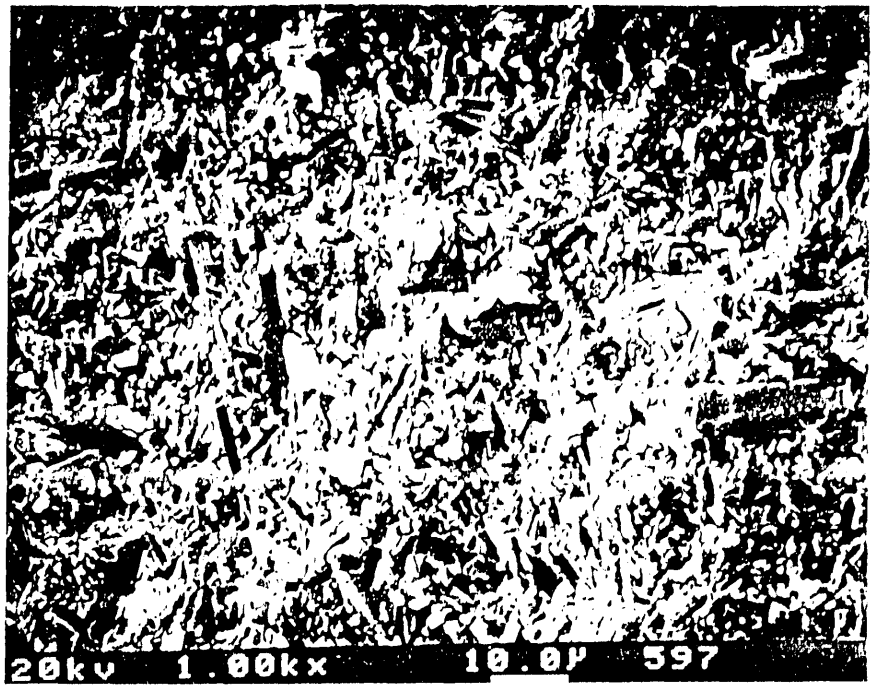

b.)

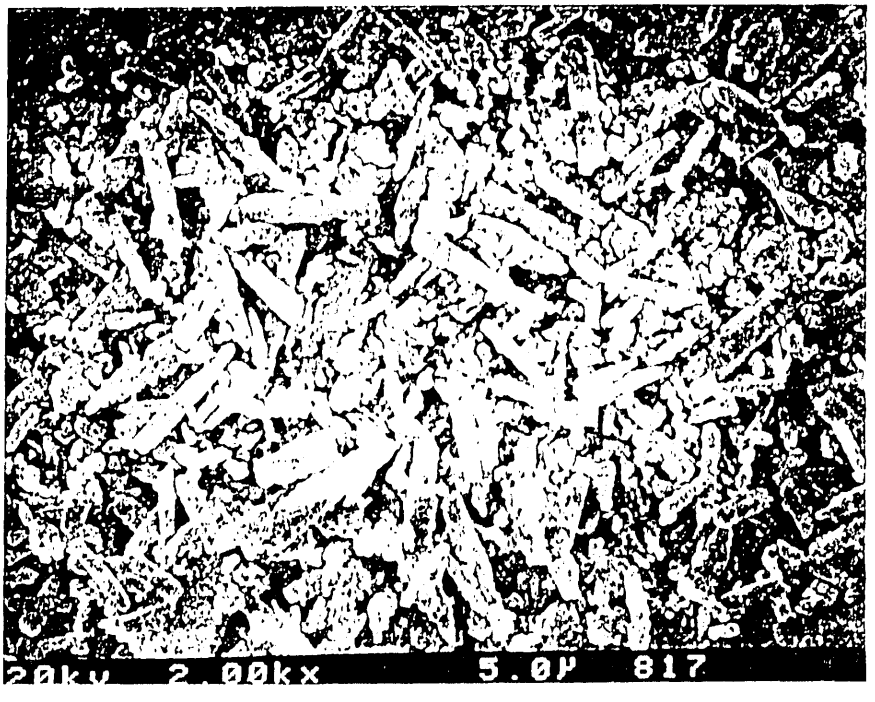

Figure 7. SEM micrographs of a.) fracture surface of as-received Si_3N_4
b.) Si_3N_4 after 19 h at 1000°C, glass etched away

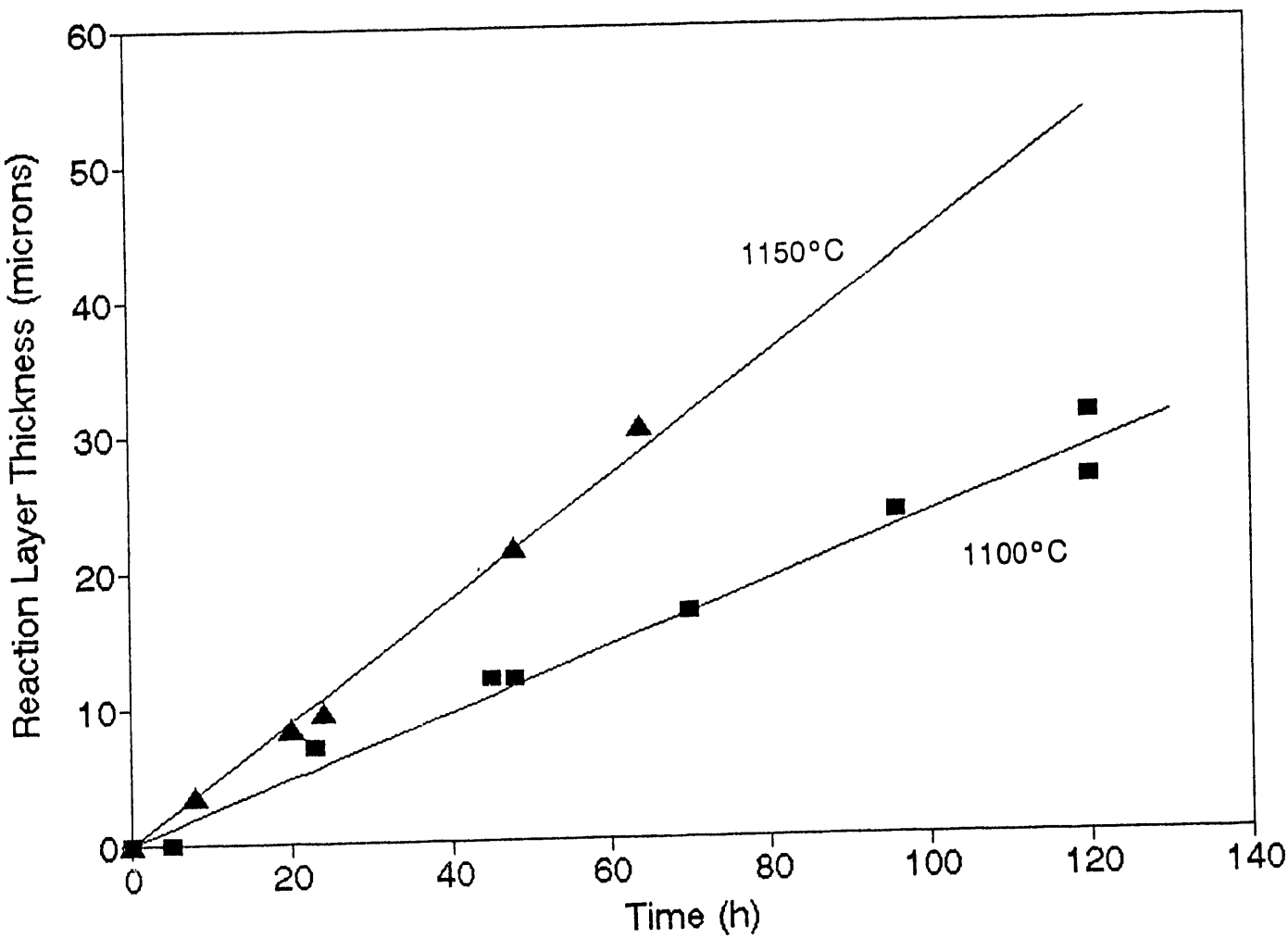

Figure 8. Alkali reaction layer thickness versus time for Al_2O_3 at 1100°C and 1150°C

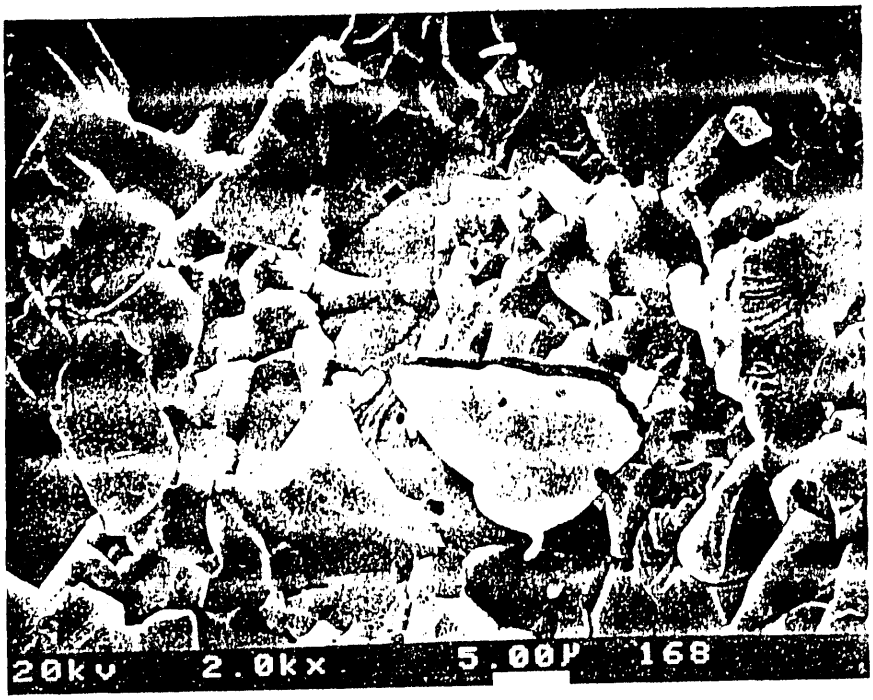

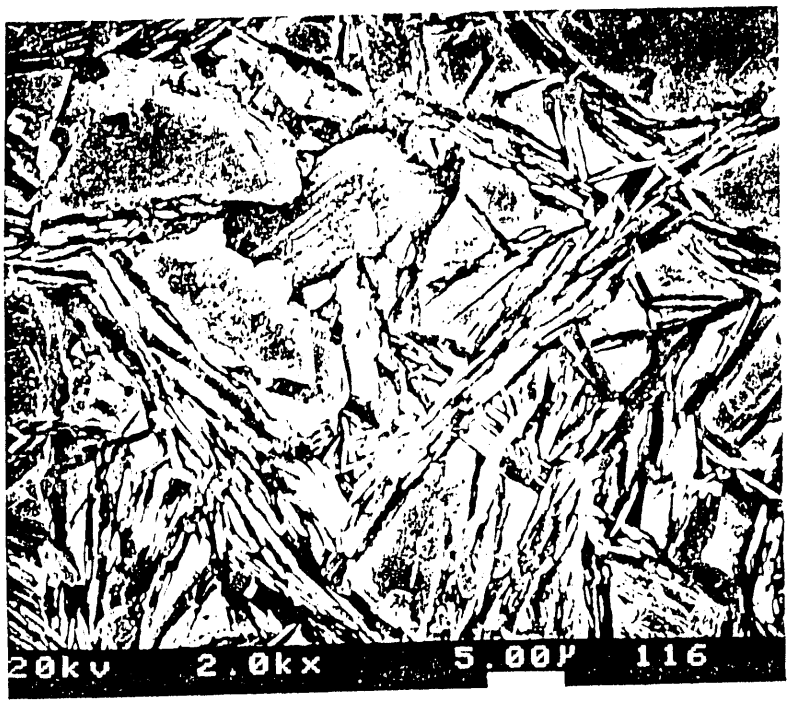

Figure 9. SEM micrographs of a.) fracture surface of as-received Al_2O_3
b.) after 120 h at 1100°C, corrosion layer etched away

DATE
FILMED
12/10/93

END